NASA/CR—2009-215672

Capillary Corner Flows With Partial and Nonwetting Fluids

D.A. Bolleddula and M.M. Weislogel
Portland State University, Portland, Oregon

September 2009

NASA STI Program . . . in Profile

Since its founding, NASA has been dedicated to the advancement of aeronautics and space science. The NASA Scientific and Technical Information (STI) program plays a key part in helping NASA maintain this important role.

The NASA STI Program operates under the auspices of the Agency Chief Information Officer. It collects, organizes, provides for archiving, and disseminates NASA's STI. The NASA STI program provides access to the NASA Aeronautics and Space Database and its public interface, the NASA Technical Reports Server, thus providing one of the largest collections of aeronautical and space science STI in the world. Results are published in both non-NASA channels and by NASA in the NASA STI Report Series, which includes the following report types:

- TECHNICAL PUBLICATION. Reports of completed research or a major significant phase of research that present the results of NASA programs and include extensive data or theoretical analysis. Includes compilations of significant scientific and technical data and information deemed to be of continuing reference value. NASA counterpart of peer-reviewed formal professional papers but has less stringent limitations on manuscript length and extent of graphic presentations.

- TECHNICAL MEMORANDUM. Scientific and technical findings that are preliminary or of specialized interest, e.g., quick release reports, working papers, and bibliographies that contain minimal annotation. Does not contain extensive analysis.

- CONTRACTOR REPORT. Scientific and technical findings by NASA-sponsored contractors and grantees.

- CONFERENCE PUBLICATION. Collected papers from scientific and technical conferences, symposia, seminars, or other meetings sponsored or cosponsored by NASA.

- SPECIAL PUBLICATION. Scientific, technical, or historical information from NASA programs, projects, and missions, often concerned with subjects having substantial public interest.

- TECHNICAL TRANSLATION. English-language translations of foreign scientific and technical material pertinent to NASA's mission.

Specialized services also include creating custom thesauri, building customized databases, organizing and publishing research results.

For more information about the NASA STI program, see the following:

- Access the NASA STI program home page at *http://www.sti.nasa.gov*

- E-mail your question via the Internet to *help@sti.nasa.gov*

- Fax your question to the NASA STI Help Desk at 443–757–5803

- Telephone the NASA STI Help Desk at 443–757–5802

- Write to:
  NASA Center for AeroSpace Information (CASI)
  7115 Standard Drive
  Hanover, MD 21076–1320

NASA/CR—2009-215672

Capillary Corner Flows With Partial and Nonwetting Fluids

D.A. Bolleddula and M.M. Weislogel
Portland State University, Portland, Oregon

Prepared under Grant NNC05AA29A

National Aeronautics and
Space Administration

Glenn Research Center
Cleveland, Ohio 44135

September 2009

Acknowledgments

This work was supported under NASA contract NNC05AA29A monitored out of NASA Glenn Research Center.

Level of Review: This material has been technically reviewed by NASA technical management.

Available from

NASA Center for Aerospace Information
7115 Standard Drive
Hanover, MD 21076–1320

National Technical Information Service
5285 Port Royal Road
Springfield, VA 22161

Available electronically at http://gltrs.grc.nasa.gov

Capillary Corner Flows With Partial and Nonwetting Fluids

D.A. Bolleddula and M.M. Weislogel
Portland State University
Portland, Oregon 97207

Abstract

Capillary flows in containers or conduits with interior corners are commonplace in nature and industry. The majority of investigations addressing such flows solve the problem numerically in terms of a friction factor for flows along corners with contact angles *below* the Concus-Finn critical wetting condition for the particular conduit geometry of interest. This research effort provides missing numerical data for the flow resistance function F_i for partially and non-wetting systems *above* the Concus-Finn condition. In such cases the fluid spontaneously de-wets the interior corner and often retracts into corner-bound drops. A banded numerical coefficient is desirable for further analysis and is achieved by careful selection of length scales x_s and y_s to nondimensionalize the problem. The optimal scaling is found to be identical to the wetting scaling, namely $x_s = H$ and $y_s = H \tan\alpha$, where H is the height from the corner to the free surface and α is the corner half-angle. Employing this scaling produces a relatively weakly varying flow resistance F_i and for subsequent analyses is treated as a constant. Example solutions to steady and transient flow problems are provided that illustrate applications of this result.

1 Introduction

The importance of capillary driven flows and phenomena has been outlined by numerous investigators [1],[2], and [3]. In this work, flows along interior corners, more accurately termed interior edges, are revisited to extend current analytical capabilities to systems exhibiting partial and non-wetting conditions. Such conditions are common to a variety of applications employing aqueous fluids such as fuel cells, flows in porous media, and waste water recycling aboard spacecraft.

1.1 Mechanism and Scope

Interior corners or edges are observed to spontaneously wick liquid into them if $\theta < \pi/2$ - α, where θ is the contact angle and α is the corner half-angle. This condition was formally

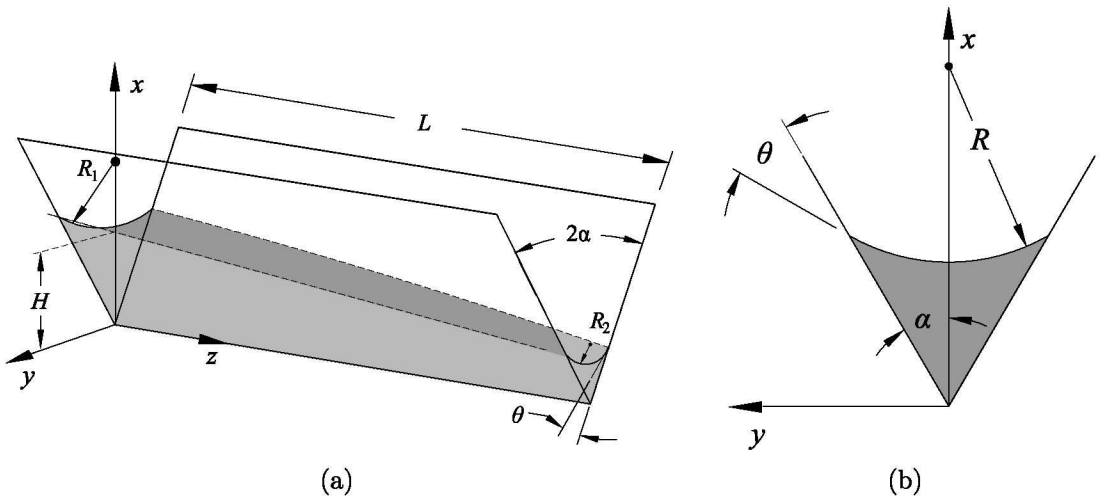

Figure 1: (a) Liquid column in an interior corner satisfying the Concus-Finn condition, $\theta < \pi/2 - \alpha$. Fluid wicks along corner in the positive z-direction. (b) Cross-flow domain of wetting corner flow

addressed by Concus and Finn [4] and is referred to in this report as the Concus-Finn condition. The mechanism for this flow is caused by a negative or favorable pressure gradient established in the wetting liquid as sketched in Fig. 1(a). The local radius of curvature is such that $R_2 < R_1$. Since the pressure drop across the liquid-gas interface is inversely proportional to R, a negative pressure gradient from position 1 to 2 results inducing a flow along the corner in the positive z-direction. When $\theta > \pi/2 - \alpha$, the curvature of the liquid-gas interface is reversed. In such partially-wetting or non-wetting conditions the fluid retracts or 'de-wets' the corner. As shown in Fig. 2(a), a positive pressure gradient in the fluid causes the fluid to flow in the negative z-direction and potentially break into drops under certain criteria [5].

Under assumptions such as a slender column, negligible inertia, and streamwise curvature, investigators such as Ayyaswamy [6], Ransohoff & Radke [7], and Romero & Yost [8] solved what is commonly referred to as the 'cross-flow' problem in the domain depicted in Fig. 1(b). Other limiting solutions for certain duct flows can also apply to the corner flow problem, i.e. rhombic duct sections Shah [9], see also White [10] for a wetting fluid in an interior corner satisfying the Concus-Finn wetting condition. Analysis of the dynamics of this flow requires the solution to the z-component Navier-Stokes equation for the velocity distribution in a 2-D section depicted in Fig. 1(b). An important aspect of the solution to this equation is the numerical coefficient that characterizes the average velocity or (flow resistance). The importance of this coefficient is revealed in subsequent solutions to dynamic flow problems of interest. All methods used by previous researchers create a coefficient that depends on the geometry to various degrees. It is observed that careful selection of geometric scales is critical to an accurate description of the flow domain and can relieve much of the numerical

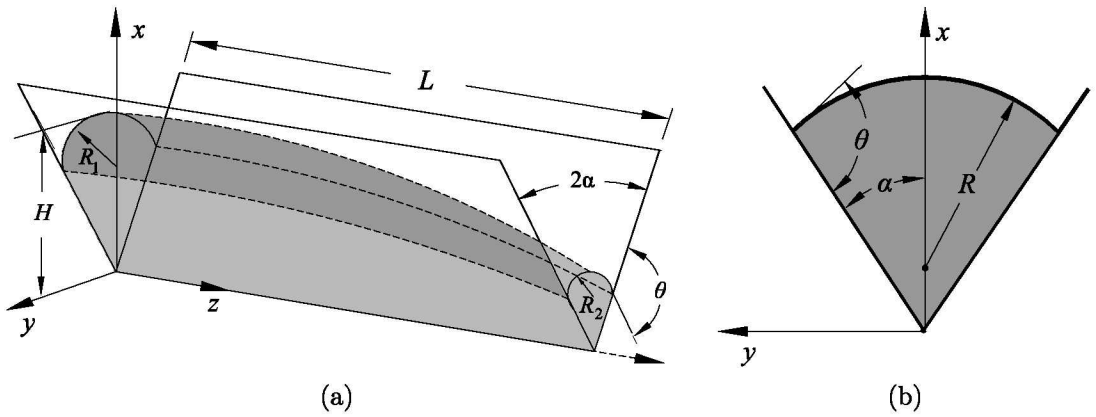

Figure 2: (a) Liquid column in an interior corner above the Concus-Finn condition, $\theta > \pi/2 - \alpha$. Fluid withdraws from the corner and flows in negative z-direction. (b) Cross-flow domain of de-wetting corner flow

dependence of the flow resistance coefficient. The scaling introduced in Weislogel and Lichter (W&L) [11] allows for a narrowly banded flow resistance function for wetted corners. The approach was predicated on assumptions such as locally parallel flows with negligible inertia.

To date, numerical methods have solved the cross-flow problem with results in terms of a flow resistance coefficient or friction factor. Ransohoff and Radke [7] identified their numerical coefficient as β while Ayyaswamy [6] determined K. Both coefficients produce undue dependence on the numerics for subsequent use in analytic solutions to more complex problems. W&L produced a narrowly banded coefficient $1/8 \lesssim F_i(\alpha, \theta) \leq 1/6$ that varies weakly on the geometry because of the choice of scales used to nondimensionalize the governing equations. Nardin [12] used the same approach for the dissimilar contact angle corner flow problem which provided a similar though slightly expanded dependence. Nardin's 2-D cross-flow problem was solved for sharp corners, rounded corners, and dissimilar wetted corners as sketched in Fig. 3. The present effort addresses de-wetting flow sections Fig. 3(d), and provides a first comprehensive solution set for all wetting scenarios. A narrowly banded numerical coefficient is desired and thus a strong emphasis is placed on identifying proper geometric length scales. The results from this study provide missing corner flow information required to solve several problems of practical concern.

The analysis begins with the reduction of the 3-D Navier Stokes equations through nondimensionalization using appropriate scales. A zeroth order Poisson equation results from the constraint of a slender column, dominant cross-stream curvature, and negligible inertia. An expanded set of non-dimensionalized variables is introduced for the reduced z-component Navier Stokes equation. The wetting flow domain is revisited with the intent of capturing optimal length scales for the de-wetting flow problem. Attention is focused on determining proper geometric length scales for the de-wetting domain in order to narrowly confine the numerical flow resistance coefficient throughout both the wetting and de-wetting flow

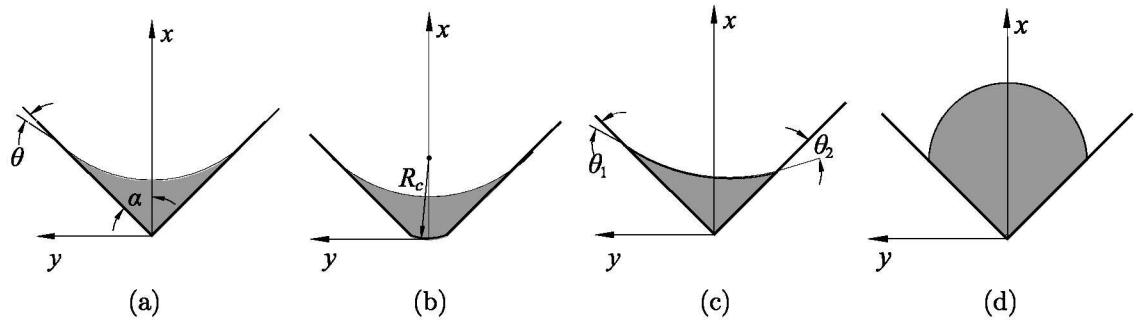

Figure 3: Interior corner cross-flow domains: (a) Sharp Corner, (b) Rounded Corner, (c) Dissimilarly Wetted Corner, and (d) De-wetting Corner

regimes. Considerable detail is presented to convey the extent of the effort made to identify the optimal scales despite the null result. Two benchmarks for the de-wetting cross-flow problem serve to verify the numerical results. Sample analytical solutions in the de-wetting regime are derived for three problems of applied interest.

It was determined after the concerted scaling effort that the wetting scaling identified in W&L provides the narrowest numerical coefficient for the de-wetting domain. This result was unexpected but is both instructive and convenient in choosing proper geometric length scales. The power of this result allows all analytic solutions previously obtained for a wetting corner to be applied to the de-wetting phenomena as well.

2 Governing Equations: Retracting Corner Flow

2.1 Analysis of Flow in an Isolated Corner

A de-wetting flow of a partial or non-wetting liquid in an isolated corner with corner half-angle α is depicted in Fig. 4. The dimensional coordinate axes are labelled with the z'-axis aligned with the corner axis. The small parameter arising in the governing equations is the slenderness ratio of the column and is defined by $\epsilon = H/L$. For the time being, the scales used in W&L for a fluid satisfying the Concus-Finn condition $\theta = \pi/2 - \alpha$ will be employed: namely that $x' \sim x_s = H$. We will report the appropriateness of this choice later. The y' length scale is perhaps not as obvious to identify and requires further consideration for the de-wetting regime. In W&L, for wetted corners, $y' \sim y_s = H \tan\alpha$ which accurately confines the cross-flow domain and produces a weakly varying numerical coefficient. A different y' length scale is expected for the flow in the de-wetting regime. By introducing the parameter T_c, which is a ratio of the y_s and x_s length scales, a degree of freedom is added such that $y_s \sim HT_c$ allowing greater flexibility in the pursuit of optimal scales.

Table 1 provides the quantities used to non-dimensionalize the governing equations. The

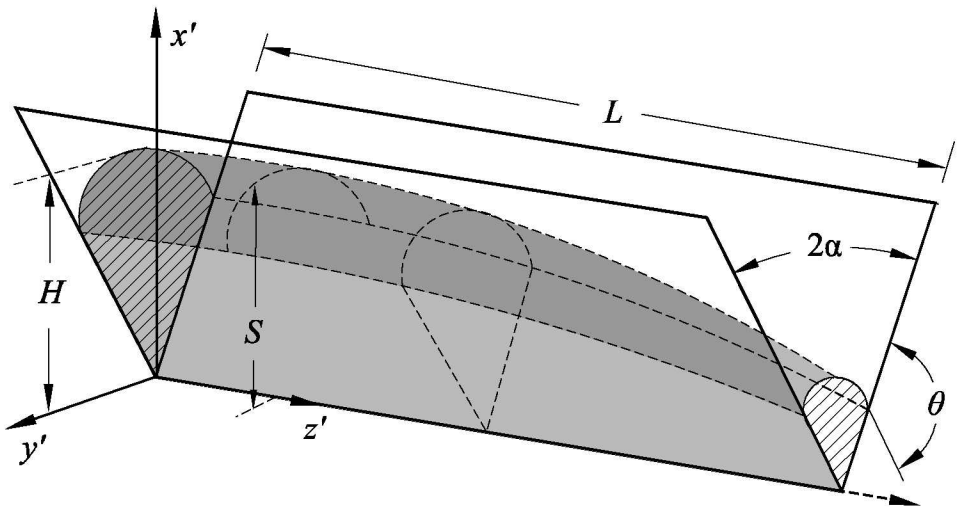

Figure 4: A liquid column in a sharp corner of angle 2α for $\theta > \pi/2$ - α. The characteristic height and length of the fluid column are H and L, respectively. The corner is 'de-wetted' by such a fluid.

Table 1: Nondimensionalized quantities where primes denote *dimensional* in/dependent variables.

Lengths	Velocities	Other
$x = x'/H$	$u = u'/\epsilon W$	$P = Hf P'/\sigma$
$y = y'/HT_c$	$v = v'/\epsilon W T_c$	$t = Wt'/L$
$z = z'/L$	$w = w'/W$	$A = A'/H^2 T_c$
$S = S'/H$	$\langle w \rangle = \langle w \rangle'/W$	$\dot{Q} = \dot{Q}'/WH^2 T_c$
$h = h'/H$	$W = \epsilon\sigma/\mu f(T_c^2/(1+T_c^2))$	$T_c = y_s/x_s$
$\mathcal{L} = \mathcal{L}'/L$		
$y_m = y'_{max}/HT_c$		

pressure is scaled using σ/Hf, where R is the radius of curvature of the free surface in the $x'-y'$ plane and f is a geometric function of proportionality between R and H that describes the curvature of the interface in the $x'-y'$ plane. The function f is accurate at zeroth order when the interface curvature along the flow direction is small, $\epsilon^2 f \ll 1$. The characteristic velocity scale in the flow direction is determined by a balance of pressure and viscous forces as shown explicitly in [13] to be

$$w' \sim W \equiv \frac{x_s^2}{\mu}\left(\frac{\partial P}{\partial z}\right)_s \left(\frac{T_c^2}{1+T_c^2}\right). \tag{1}$$

Substitution of the non-dimensional quantities in Table 1 into the individual component

equations of Navier-Stokes gives[†]

$$\epsilon^2 \mathcal{R} \frac{\mathrm{D}u}{\mathrm{D}t} = -P_x + \epsilon^2 \nabla^2 u, \tag{2}$$

$$\epsilon^2 \mathcal{R} T_c^2 \frac{\mathrm{D}v}{\mathrm{D}t} = -P_y + \epsilon^2 T_c^2 \nabla^2 v, \tag{3}$$

and

$$\mathcal{R} \frac{\mathrm{D}w}{\mathrm{D}t} = -P_z + \nabla^2 w, \tag{4}$$

where

$$\frac{\mathrm{D}}{\mathrm{D}t} \equiv \frac{\partial}{\partial t} + u\frac{\partial}{\partial x} + v\frac{\partial}{\partial y} + w\frac{\partial}{\partial z}, \tag{5}$$

and in the limit of $\epsilon^2 \ll 1$

$$\nabla^2 \equiv \frac{T_c^2}{1+T_c^2}\frac{\partial^2}{\partial x^2} + \frac{1}{1+T_c^2}\frac{\partial^2}{\partial y^2} + \epsilon^2 \frac{T_c^2}{1+T_c^2}\frac{\partial^2}{\partial z^2}, \tag{6}$$

and

$$\mathcal{R} = \frac{\epsilon^2}{f} Su \left(\frac{T_c^2}{1+T_c^2} \right)^2. \tag{7}$$

The parameter $Su = \sigma \rho H / \mu^2$ is the Suratman number and provides a measure of inertia in the flow. For many terrestrial corner flow tests $Su \sim O(1)$, however $Su \gg 1$ is common in the low-g environments provided in drop tower tests ($Su \sim O(10^4)$).

The continuity equation is

$$\nabla \cdot \mathbf{v} = 0. \tag{8}$$

The boundary conditions for the system of equations are no slip along the walls and zero shear stress on the free surface. For a complete listing of the transverse and normal shear stress conditions see [14].

2.2 Asymptotic equations

The governing equations are greatly simplified by an asymptotic method employing the slenderness ratio ϵ as the small parameter. In what is frequently referred to as the lubrication

[†]Subscript notation on pressure terms denote differentiation with respect to designated variable.

approximation for slender fluid columns where $\epsilon^2 \ll 1$ and $\mathcal{R} \lesssim O(\epsilon^2)$, the Navier-Stokes equations reduce to the single zeroth order z-component equation

$$\frac{\partial P}{\partial z} = \frac{T_c^2}{1+T_c^2}\frac{\partial^2 w}{\partial x^2} + \frac{1}{1+T_c^2}\frac{\partial^2 w}{\partial y^2}, \tag{9}$$

where $T_c \equiv y_s/x_s$ alluded to in § 2.1. Equation 9 is referred to as the dimensionless cross-flow problem and describes the velocity distribution of the fluid in any cross-flow section. With the added flexibility provided by T_c, a variety of potential length scales can be tested systematically with relative ease. The utility of this parameter will become apparent as numerous scales were investigated while only a sample are presented. As necessary background, the scaling employed by W&L for wetting corners is reviewed first. The de-wetting cross-flow sections are then presented, solved, and optimal scalings pursued.

2.3 Wetting Formulation

For corner flows with wetting fluids the length scales $x_s = H$ and $y_s = H\tan\alpha$ are such that $T_c \equiv \tan\alpha$ and Eq. 9 simplifies to

$$\frac{\partial P}{\partial z} = \frac{\partial^2 w}{\partial x^2}\sin^2\alpha + \frac{\partial^2 w}{\partial y^2}\cos^2\alpha, \tag{10}$$

subject to no slip on the walls

$$w = 0 \qquad \text{on} \qquad y = \pm x, \tag{11}$$

and no shear on the free surface

$$\frac{\partial w}{\partial x} - \frac{\partial S}{\partial y}\frac{\partial w}{\partial y}\cot^2\alpha = 0 \qquad \text{on} \qquad x = S. \tag{12}$$

Under the assumptions of a slender column $\epsilon^2 \ll 1$ and negligible transverse surface curvature $\epsilon^2 f \ll 1$, the free surface $S(y,z,t)$ is defined as a construct of circular arcs in $x-y$ planes satisfying the contact angle condition at the wall. In the dimensionless domain the free surface is given by

$$S(y,h) = h(1+f) - \left(h^2 f^2 - y^2\tan^2\alpha\right)^{1/2}, \tag{13}$$

where $0 \le y \le y_m$ and

$$f = \frac{\sin\alpha}{\cos\theta - \sin\alpha}. \tag{14}$$

The governing Navier-Stokes equation under the assumptions described above are solved for the z-component velocity distribution $w(x,y,z,t)$. The dimensionless average velocity $\langle w\rangle = \langle w\rangle(z,t)$ is expressed as

$$\langle w \rangle = -F_i h^2 \frac{\partial P}{\partial z}, \tag{15}$$

where

$$\frac{\partial P}{\partial z} = \frac{1}{h^2} \frac{\partial h}{\partial z}, \tag{16}$$

and where F_i is the numerically solved coefficient formally defined as

$$F_i = \frac{x_s y_s}{A'} \int \int w \, dx \, dy. \tag{17}$$

The dynamics of a wetting or de-wetting flow in a corner is governed by the global mass balance equation:

$$\frac{\partial A}{\partial t} = -\frac{\partial}{\partial z}(A\langle w \rangle), \tag{18}$$

where the dimensionless area is

$$A = h^2 F_A / \tan \alpha, \tag{19}$$

with

$$F_A = f^2 \left(\frac{\sin \delta \cos \theta}{\sin \alpha} - \delta \right). \tag{20}$$

F_A is a dimensionless area function determined by the cross flow geometry. Upon substitution of A and the average velocity given by Eq. 15, the leading order governing equation becomes

$$\frac{\partial}{\partial t} \left[\frac{h^2 F_A}{\tan \alpha} \right] = -\frac{\partial}{\partial z} \left[\frac{h^2 F_A}{\tan \alpha} \left(-F_i \frac{\partial h}{\partial z} \right) \right]. \tag{21}$$

The dimensionless cross-flow problem modeled by Eqs. (10)-(12) is solved in the domain sketched in Fig. 5(b). It is important to note the transformation that takes place from the dimensional domain depicted in Fig. 5(a) to the dimensionless domain Fig. 5(b). The walls in the dimensionless domain are locked at $\pi/4$ regardless of the corner angle α. Also the free surface is stretched into a portion of an ellipse instead of a circle. The dimensionless coefficient $F_i(\alpha,\theta)$ is determined numerically but is confined for all values of α and θ due to the choice of length scales x_s and y_s. For all values of α and θ satisfying the Concus-Finn condition $\theta \leq \pi/2$ - α, $1/8 \lesssim F_i \leq 1/6$. In fact it can be shown that much of this limited dependence is due to α and that $F_i = 1/6(1 - 1/5 \sin 2\alpha)$ provides a fair correlation of $F_i \pm$ 2.5% in the wetting regime (note this correlation is devoid of θ-dependence. Conditions for which $\theta \geq \pi/2$ - α above this range have not yet been studied by our research group, nor to our knowledge in the literature. It is intended that a physically motivated choice of scales

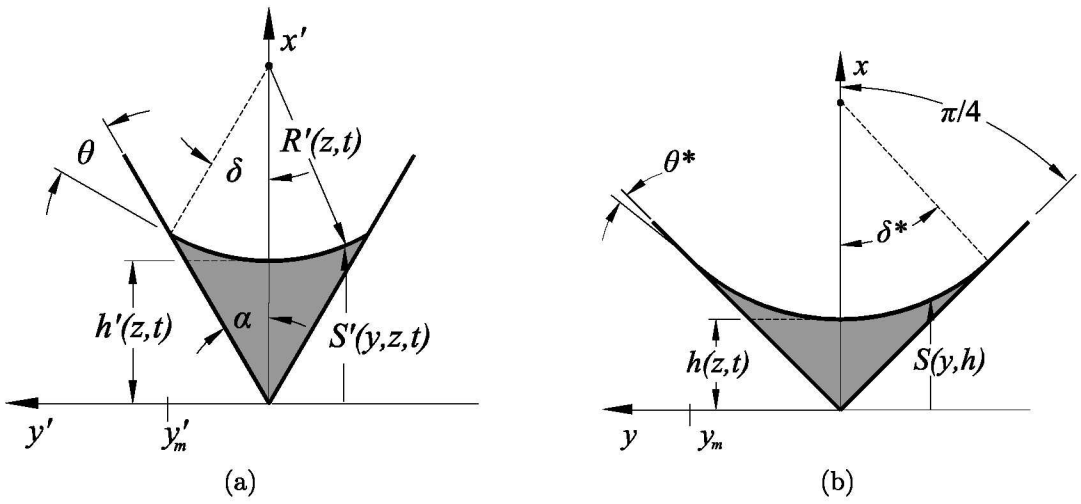

Figure 5: (a) Schematic of dimensional cross section for $\theta \leq \pi/2$ - α. (b) Dimensionless cross-flow area for $x \sim H$ and $y \sim H\tan\alpha$. The fluid surface intersects the wall at $y_m = hf$ sin δ cot α where $\delta = \pi/2$ - α - θ. The contact angle θ and the interface curvature angle δ appear as $\theta^* = \pi/4$ - $\tan^{-1}(\tan\alpha \tan\delta)$ and $\delta^* = \tan^{-1}(\sin\delta \cos\alpha/(\cos\theta$ - $\cos\alpha \sin\delta))$.

for the de-wetting domain will confine F_i to a similar, narrowly banded coefficient as for the wetting case. It is not clear a priori which choice of scaling will provide this behavior for F_i. However, if F_i can be confined to a narrow band, further theoretical analysis for de-wetting flows can proceed directly.

2.4 De-wetting Formulation

The remainder of this report addresses the de-wetting problem where

$$\pi/2 - \alpha \leq \theta \leq \pi \tag{22}$$

Figure 6(a) provides a typical section of the corner flow. The key geometric parameters of the problem are α, θ, and δ, where $\delta = \pi/2$ - α - θ. The length scales for the wetting cross-sections are used initially before other scales are employed. This provides a benchmark for F_i values in the limiting case of $\theta \searrow \pi/2 - \alpha$. An interesting aspect of the de-wetting cross-section is that the curvature function f naturally changes sign across the Concus-Finn critical wetting condition of $\theta = \pi/2$ - α. This sign change directly affects only one function in the cross-flow problem Eqs. (10)-(12). The equation that defines the free surface incorporates a sign function on f in front of the square root term specifying the top(+) or bottom(-) half of the circular arc. The dimensionless free surface function is defined below for the geometry shown in Fig. 6(b),

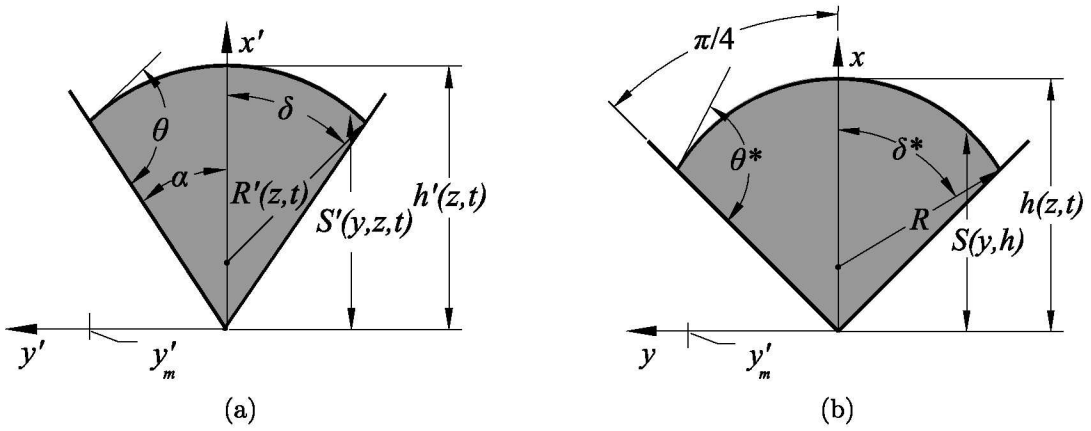

Figure 6: (a) Schematic of dimensional cross section when $\theta \geq \pi/2$ - α. (b) Dimensionless cross-flow area where $\theta^* = \pi/4 + \tan^{-1}(\text{-tan } \alpha \text{ tan } \delta)$ and $\delta^* = \tan^{-1}(\sin \delta \cos \alpha/(\cos \theta + \cos \alpha \sin \delta))$

$$S(y,h) = h(1+f) - \text{sgn}(f)\left(h^2 f^2 - y^2 \tan^2 \alpha\right)^{1/2}. \tag{23}$$

The cross-sectional area is represented by $A' = h'^2 F_A$. It is interesting to note that the dimensionless area function F_A is identical for both wetting (Fig. 5) and de-wetting (Fig. 6) cross-sections[‡].

It seems intuitive that $x_s = H$ should be a reasonable choice to normalize the height of the interface h. However the choice of y_s is complicated by the various limits of the geometry. For example, if $y_s = H \tan \alpha$, y_s falls outside the cross-flow section seen in Fig. 7. However, as α approaches $\pi/2$, then $y_s \longrightarrow \infty$ and guarantees that gradients in the flow are limited to the x'-direction as expected. Although this fact appears to characterize the limits of the geometry for this problem, a systematic optimization of scales is warranted.

3 Numerical Results, F_i

3.1 Scaling

A well selected scaling should confine the physical domain and accurately represent the governing equations for the limits of the problem. Here we pursue scaling that confines the cross-sectional area in the wetting and de-wetting cases as well as solve cross-flow equations accurately for all geometrical limits. For the cross-sections studied the contact angle is

[‡]For clarity in reference to the cross-flow domain, wetting and de-wetting cross sections are defined here when the free surface is concave up (positive curvature) and concave down (negative curvature), respectively.

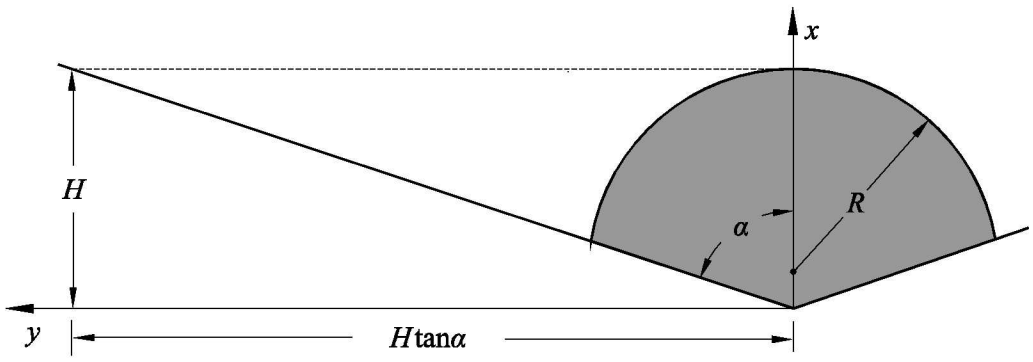

Figure 7: Depiction of wetting scaling $x_s = H$ and $y_s = H \tan \alpha$ on a large corner angle de-wetting section.

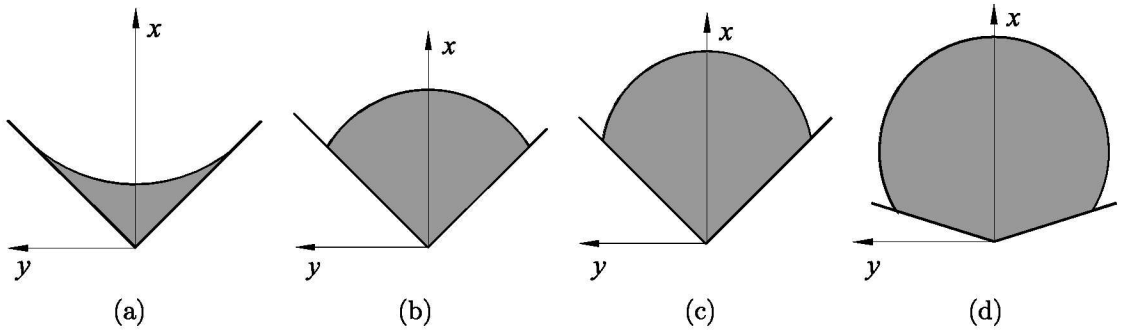

Figure 8: Characteristic corner flow cross-sections to cross-flow problems. (a) characteristic wetting cross-section when $\theta \leq \pi/2$ - α. (b) De-wetting cross-section with acute θ, $\pi/2$ - α $\leq \theta \leq \pi/2$. (c) De-wetting cross-section with obtuse θ, $\pi/2 \leq \theta \leq \pi$ - α. (d) De-wetting cross-section with highly obtuse θ, π - $\alpha \leq \theta \leq \pi$, or 'non-wetting' systems where $\theta > \pi/2$.

divided into the four types specified in Fig. 8. The wetting cross-sections have been studied extensively for sharp corners [6] and rounded corners [15].

An effort here is made to determine optimal length scales for the wetting and de-wetting cross sections. Wetting sections are revisited in this study with hopes of confining F_i to a narrower band. This process involves determining the correct combination of x' and y' length scales such that F_i can be narrowly banded and treated as a constant in the governing evolution Eq. 21 for more important solutions to follow.

Figure 9 depicts various geometrically motivated length scales chosen to determine if F_i can be more accurately confined for the wetting and de-wetting sections. Before discussing the results of F_i employed with various length scales, a brief description of the numerical procedure will be outlined.

The numerical results (F_i) are obtained using MATLAB® implementing a finite element method. The final solution is obtained after the initial mesh is adaptively refined

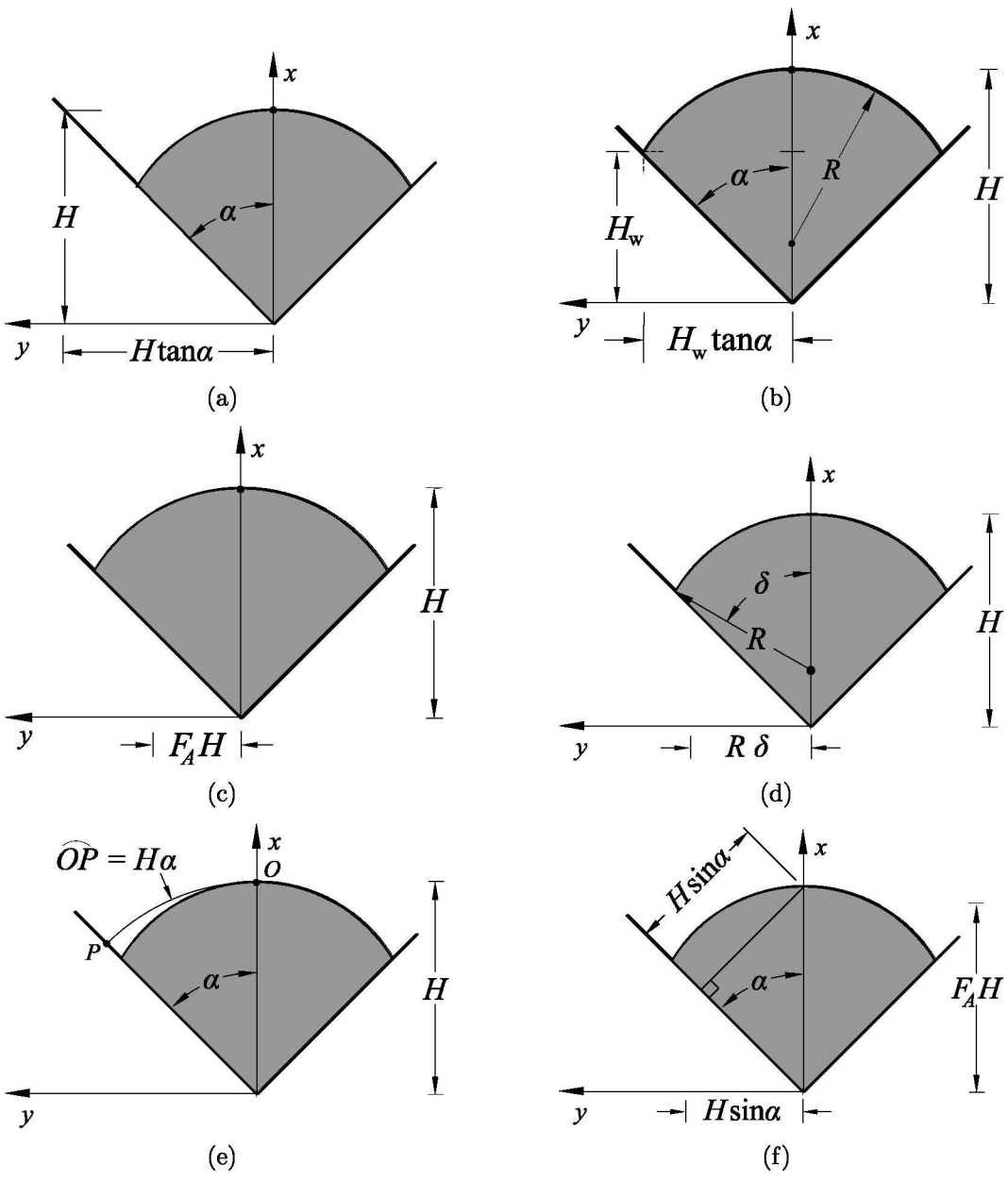

Figure 9: Depiction of various x_s and y_s: (a) $x_s = H$ and $y_s = H \tan\alpha$, (b) $x_s = H$ and $y_s = H_w \tan\alpha$, (c) $x_s = H$ and $y_s = F_A H$, (d) $x_s = H$ and $y_s = R\delta$, (e) $x_s = H$ and $y_s = H\alpha$, and (f) $x_s = F_A H$ and $y_s = H \sin\alpha$.

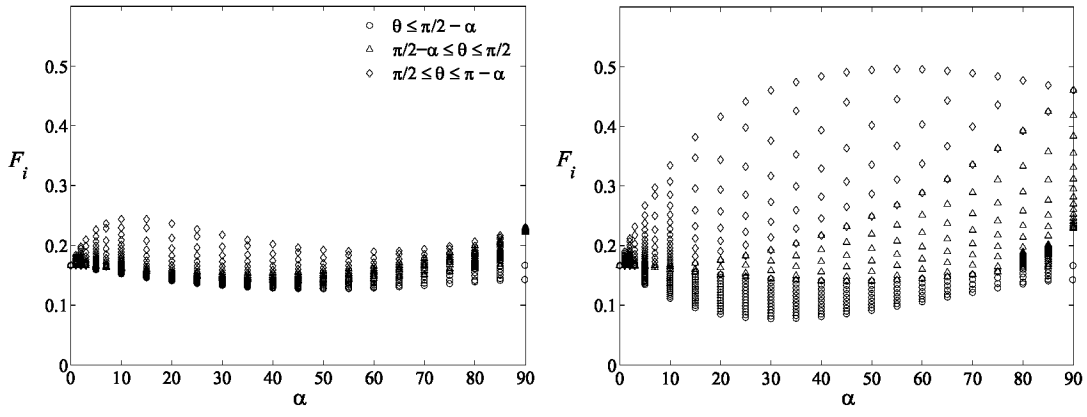

(a) $x_s = H$ and $y_s = H \tan\alpha$

(b) $x_s = H$ and $y_s = H_w \tan\alpha$

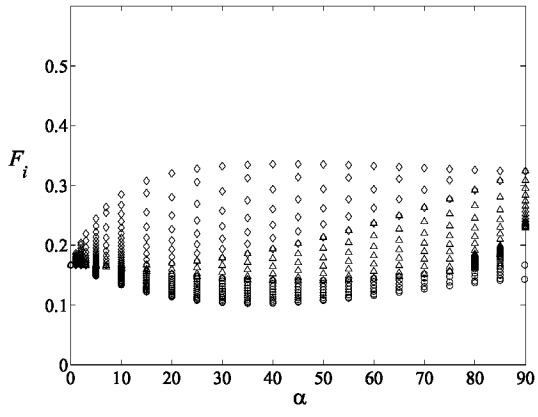

(c) $x_s = H$ and $y_s = F_A H$

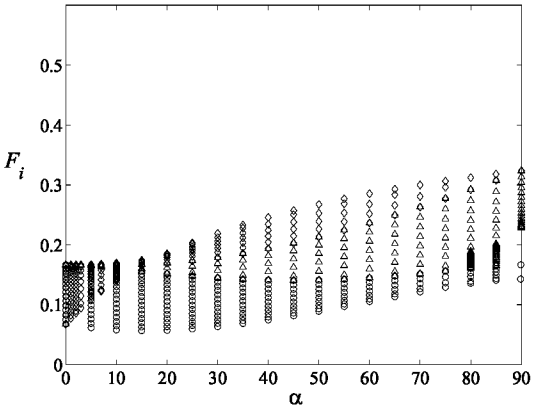

(d) $x_s = H$ and $y_s = R\delta$

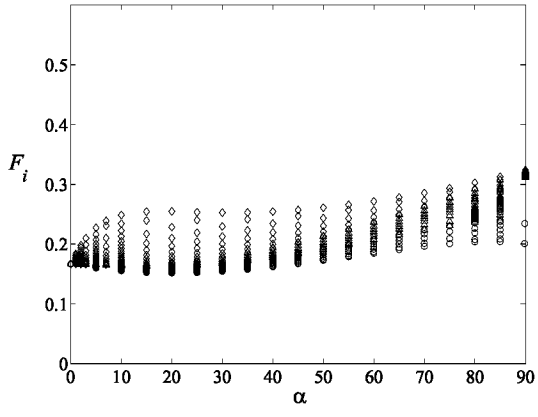

(e) $x_s = H$ and $y_s = H\alpha$

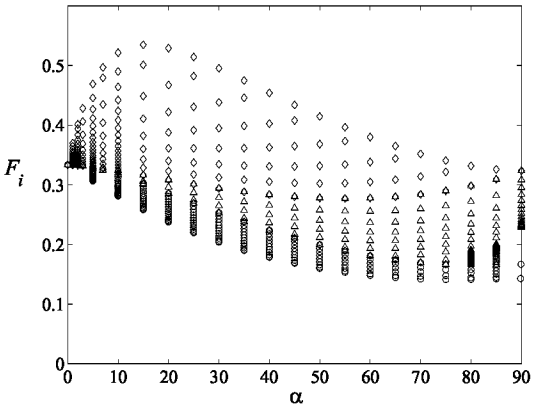

(f) $x_s = F_A H$ and $y_s = H \sin\alpha$

Figure 10: Plot of F_i for various scales. The legend in Fig. (a) identifies regimes circles for $\theta \leq \pi/2$ - α, triangles for $\pi/2$ - $\alpha \leq \theta \leq \pi/2$, and diamonds for $\pi/2 \leq \theta \leq \pi$ - α.

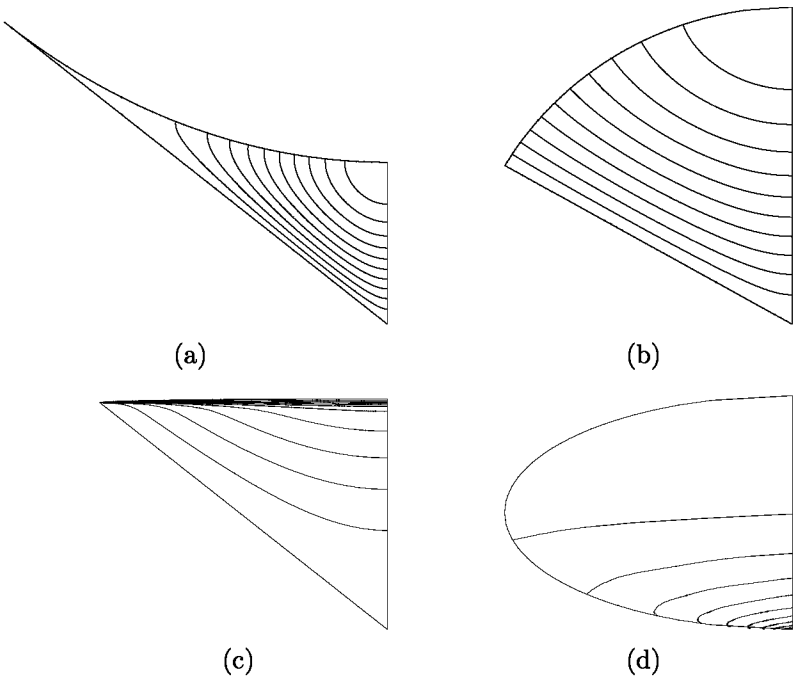

Figure 11: Contour plots from numerical solution: (a) $\alpha = 60°$and $\theta = 0°$ (b) $\alpha = 60°$and $\theta = 90°$ (c) $\alpha = 1°$and $\theta = 180°$, and (d) $\alpha = 90°$and $\theta = 180°$

until convergence is achieved. All F_i's computed have 50,000-60,000 elements. Run time is approximately three minutes for each computation of F_i using a 1.86 GHz AMD Athlon, running XP2500+. Figure 10 shows F_i scaled with the corresponding length scales in Fig. 9. It is immediately obvious from Fig. 10(a) that the wetting scaling confines F_i to the highest degree. Figure 11 shows select contour plots from the numerical output.

It must be made clear that the scaling identified in Fig. 9(a) and 9(b) was employed and solved in separate numerical codes at the resolution specified above. In this report, the numerical values presented are computed employing the scaling in Fig. 9(a). It can be shown that all other results may be and thus are determined through the following transformation

$$\left[F_i\left(\frac{T_c^2}{1+T_c^2}\right)\right]_1 = \left[F_i\left(\frac{T_c^2}{1+T_c^2}\right)\right]_2 \tag{24}$$

F_i's investigated are determined by solving Eq. 24 for $[F_i]_2$ shown explicitly to be

$$[F_i]_2 = \frac{\left[F_i\left(\frac{T_c^2}{1+T_c^2}\right)\right]_1}{\left(\frac{T_c^2}{1+T_c^2}\right)_2} \tag{25}$$

The numerically computed F_i is identified by the subscript 1 while the desired F_i is denoted

by 2. Thus the F_i pursued is found through a ratio of x_s and y_s length scales multiplied by the computed F_i denoted by the subscript 1. At this point it should be appreciated how the parameter T_c provides flexibility in the pursuit of optimal scaling.

The forgoing discussion refers only to F_i computed for $0 \leq \theta \leq \pi - \alpha$. A variety of length scales are attempted but the six identified in Fig. 9 identify the most insightful and physically motivated choices. When $x_s = H$ and $y_s = H \tan\alpha$, the wetting cross-section is accurately confined as depicted in Fig. 9(a), while only neglecting a narrow portion of the flow area where negligible flow is present. If this same idea is applied to the de-wetting cross-sections then $x_s = H$ and $y_s = H_w \tan\alpha$ would make a good choice of length scales, 9(b). Perhaps surprisingly, this actually creates a wider spread of F_i as seen in Fig. 10(b). Other length scales shown in Figs. 9 (c)-(f) are attempted and motivated by the geometry of the flow domain keeping in mind the limits of α and θ, but none to date provide a tighter banding of F_i. It is clear by inspection of Fig. 10(a) that this choice confines F_i to a narrower band. Figure 10(e) shows the results when $x_s = H$ and $y_s = H\alpha$ which bands F_i effectively for $\alpha \lesssim 40°$ but the collapse is lost for $\alpha \gtrsim 40\,°$. In an attempt to verify the appropriateness of $x_s = H$, a choice motivated by the area function was implemented. Figure 10(f) has $x_s = F_A H$ and $y_s = H \sin\alpha$. This again did not provide a tighter bound on F_i. It was originally anticipated that the wetting scaling was neither physical or optimal for the de-wetting cross-sections, but after numerous combinations of x_s and y_s, length scales $x_s = H$ and $y_s = H \tan\alpha$ appear to provide the tightest confinement of F_i for both the de-wetting and wetting cross-sections. One reason for this is seen in the limits of governing Eq. 10. When $\alpha \longrightarrow 0$, the w_{xx} derivative term becomes insignificant, similarly when $\alpha \longrightarrow \pi/2$, the w_{yy} term vanishes. Currently this behavior is believed to confine F_i to the highest degree for the de-wetting sections.

3.2 Benchmark: Fully Developed Laminar Duct Flow

To confirm the numerical procedure and results for the computation of F_i, the technique is compared to an exact analytical solution for flow through a circular sector duct found in White [10]. A no slip boundary condition is applied to the boundary identifying the free surface in the cross-flow formulation and F_i is computed for $0 \leq \alpha \leq \pi/2$ with $\theta = \pi/2$. The exact solution of flow through a circular sector duct is presented in terms of the average velocity as follows,

$$\langle w \rangle_{exact} = -\frac{f}{2\alpha}\left(\frac{1+T_c^2}{T_c^2}\right)\left[\frac{\tan\alpha - \alpha}{4} - \frac{32\alpha^4}{\pi^5}\sum_{i=1,3,5}^{\infty}\frac{1}{i^2(i+2\alpha/\pi)^2(i-2\alpha/\pi)}\right]\frac{\partial h}{\partial z}, \quad (26)$$

where the terms multiplied by $\partial h/\partial z$ on the right hand side of Eq. 26 are equivalent to F_i with $T_c = \tan\alpha$. The modified Poisson equation 10 is solved numerically and integrated over the domain to determine the dimensionless average velocity from which F_i can be compared to the exact solution, $F_{i_{exact}}$.

Figure 12 shows excellent agreement for all α with results accurate to 4 digits. The numerical code thus verifies its utility and implementation for the de-wetting corner cross-flow problem. The numerical code also verifies wetting corner flow benchmarks listed in [16] with accuracy to $\pm 0.5\%$ or better, i.e. $F_i = 1/6$ as $\alpha \longrightarrow 0$ first shown in [14].

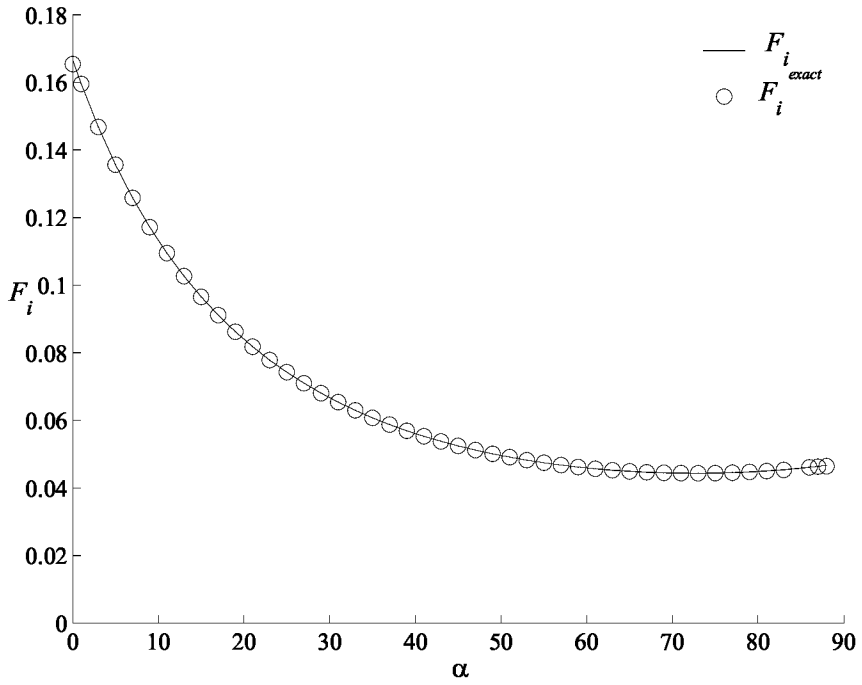

Figure 12: Comparison of exact solution of fully developed laminar flow through a circular sector duct compared to numerical solution

3.3 F_i Summary

An accurate numerical procedure to compute F_i was detailed in § 3.2. In § 3.1 an optimal scaling for the wetting cross-sections is also acceptable and perhaps best for the de-wetting cross-sections too. For the wetting cross-sections $1/8 \lesssim F_i \leq 1/6$ and achieves a $\pm 14\%$ error when $F_i \approx 1/7$. For the de-wetting cross-sections $0.141 \lesssim F_i \lesssim 0.244$ with a $\pm 27\%$ error when $F_i \approx 0.192$ with $\pi/2 - \alpha \leq \theta \leq \pi - \alpha$. Over 700 values are computed and shown in Fig. 13. Figure 14 shows F_i versus α where $\pi - \alpha \leq \theta \leq \pi$. For this 'non-wetting' regime F_i is not nearly as confined but the wetting scaling still provides the tightest bound given the limits of the cross-flow geometry. A complete catalogue of F_i for given corner-half angle α and contact angle θ is provided in the Appendix.

It is clear that the range of F_i values for the de-wetting corner sections expands compared to the wetting sections and in particular for the non-wetting regime where $\theta > \pi/2$. However, $x_s = H$ and $y_s = H \tan\alpha$ appear to be the optimal scales identified to date. This result was not expected a priori, but is appreciated in retrospect as analytical solutions obtained by

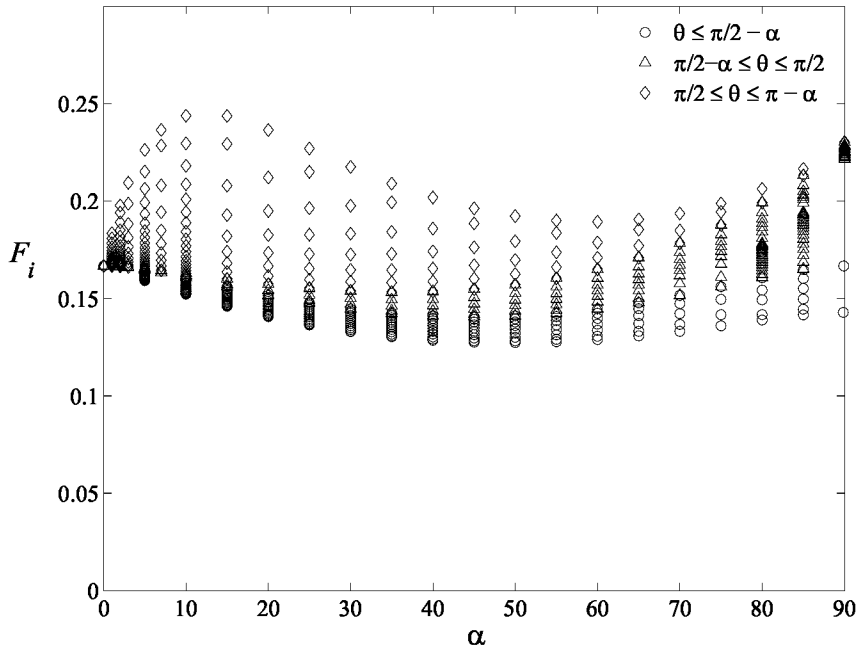

Figure 13: $F_i(\alpha, \theta)$. F_i is plotted for $0 \leq \alpha \leq \pi/2$ in the wetting sections $\theta \leq \pi/2 - \alpha$ and two de-wetting regimes $\pi/2 - \alpha \leq \theta \leq \pi/2$ and $\pi/2 \leq \theta \leq \pi - \alpha$

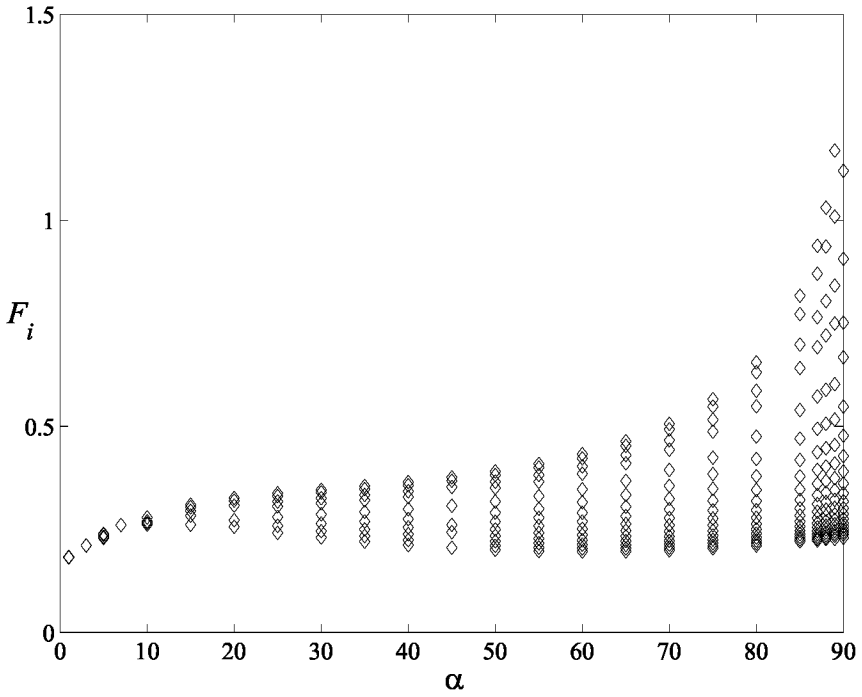

Figure 14: $F_i(\alpha, \theta)$. F_i is plotted for $0 \leq \alpha \leq \pi/2$ in the third, non-wetting regime where $\pi - \alpha \leq \theta \leq \pi$

previous investigators can be recovered since identical scaling accounts for both the wetting and de-wetting corner flow cross-sections.

Since F_i is computed and the error associated with treating it as a constant is known, the governing equation arising from the global mass balance can be solved applicable to a variety of flow scenarios.

4 Analytic Solutions: De-Wetted Corners

4.1 Steady Solution

Many interesting and potentially applicable analytical solutions to Eq. 21 can be found. Several important ones are presented here. First by noting that F_A and F_i are not functions of z and by introducing the transformation $\tau = F_i t/2$, the governing evolution equation reduces to

$$\frac{\partial h}{\partial \tau} = 2\left(\frac{\partial h}{\partial z}\right)^2 + h\frac{\partial^2 h}{\partial z^2}. \tag{27}$$

The steady solution to Eq. 27 is

$$h = (B_1 + B_2 z)^{1/3} \tag{28}$$

where B_1 and B_2 are constants of integration which can be determined by specified boundary conditions. By specifying $h(z_1,\tau)=H_1$ and $h(z_2,\tau)=H_2$ and solving Eq. 28, the steady capillary flow rate for a fluid of column length $\mathcal{L}$ can be found. The steady solution expressed in dimensionless form by Eq. 28 for the case of $h(0) = H_1$ and $h(\mathcal{L}) = H_2$ is expressed dimensionally as

$$h' = \left(H_1^3 - (H_1^3 - H_2^3)\frac{z}{\mathcal{L}}\right)^{1/3} \tag{29}$$

and

$$\dot{Q}' = \frac{F_i F_A \sigma \sin^2\alpha}{3\mu f \mathcal{L}}\left(H_1^3 - H_2^3\right). \tag{30}$$

This solution is identical to that presented in [14] for the wetting problem, only the flow retraction is seen through the curvature function f as it changes sign above the Concus-Finn condition.

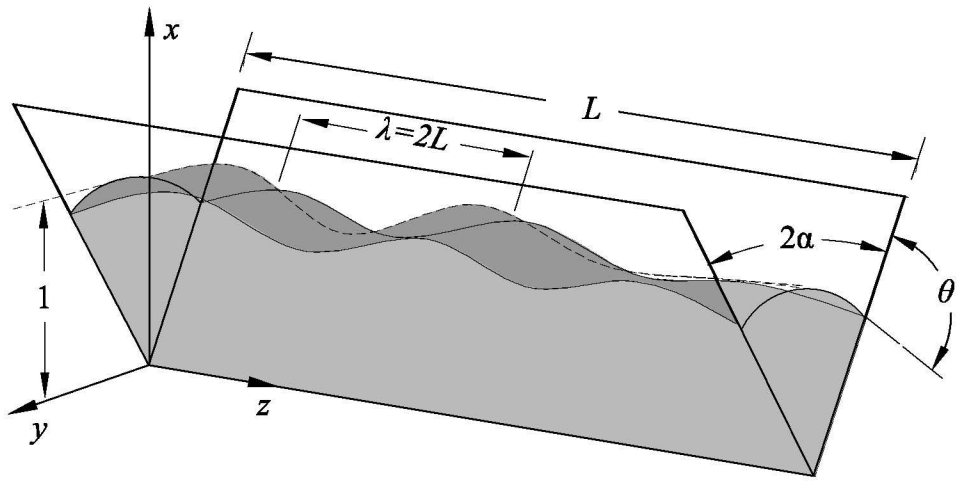

Figure 15: Isometric view of flow in a corner with a convex free surface and sinusoidal perturbation applied to the free surface.

4.2 Infinite Column Solution

This problem describes the motion of a slightly perturbed liquid column in an interior corner originally addressed in [14]. This problem is approached with an asymptotic analysis where the disturbance is modeled by a sinusoidal perturbation of the axial meniscus centerline height h, as in Fig. 15. A regular asymptotic expansion for h is

$$h = h_0 + \epsilon h_1 + \epsilon^2 h_2 + \ldots \tag{31}$$

Substituting 31 into Eq. 27 yields the $O(1)$ equation

$$\frac{\partial h_0}{\partial \tau} = 2\left(\frac{\partial h_0}{\partial z}\right)^2 + h_0 \frac{\partial^2 h_0}{\partial z^2} \tag{32}$$

and the $O(\epsilon)$ equation is

$$\frac{\partial h_1}{\partial \tau} = 4\frac{\partial h_0}{\partial z}\frac{\partial h_1}{\partial z} + h_0 \frac{\partial^2 h_1}{\partial z^2} + h_1 \frac{\partial^2 h_0}{\partial z^2}, \tag{33}$$

If $h_o = const$ is a solution to Eq. 32 then it describes a uniform height interface at steady state. Solving Eq. 33 to $O(\epsilon)$ results with an asymptotic sequence shown as

$$h = h_0 + \epsilon C_4 \exp[-\lambda^2 h_0 \tau] \cos(\lambda z + C_5) + O(\epsilon^2) \tag{34}$$

where λ is the dimensionless wave number ($\lambda = \lambda'/L$) of some perturbation to the column of fluid and C_4 and C_5 are constants determined by the boundary conditions. The main difference between the wetting regime and the de-wetting regime solutions can be seen through redimensionalization of the time constant in the exponent,

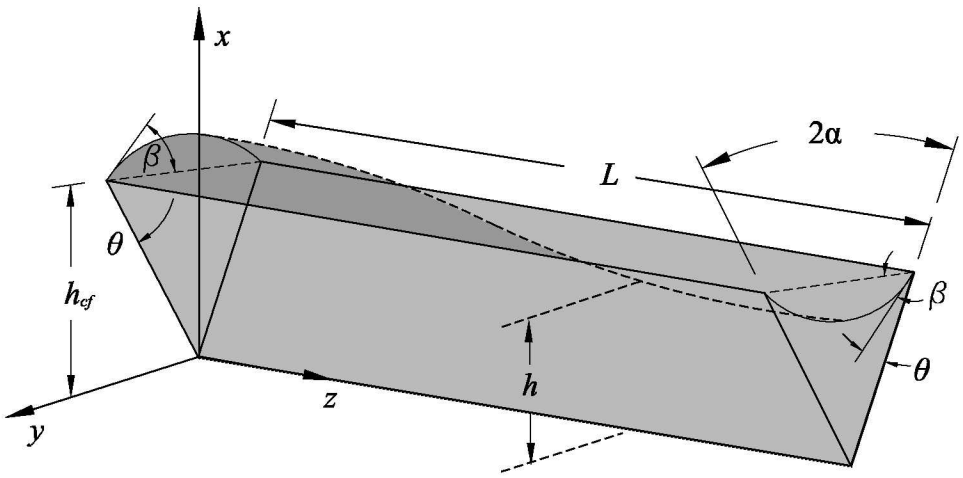

Figure 16: Isometric view of a fluid pinned along the edges of a corner where in the inlet is perturbed *above* and *below* the Concus-Finn condition, respectively.

$$\lambda^2 h_0 \tau \sim \epsilon^2 \frac{F_i \sin^2 \alpha}{f} \frac{\sigma t}{\mu H}. \tag{35}$$

Since the sign of f is negative in the de-wetting regime, the solution is unstable as the exponent is positive leading to exponential growth of the perturbation. The behavior in the solution verifies the instability of a liquid column in a corner identified by Langbein [5]. The criteria is defined when the length of the column $L \geq 2\pi R$ ($R = Hf$), upon which the liquid column will break into drops to achieve a lower energy state.

4.3 Axially Perturbed Interface Solution

The scenario depicted in Fig. 16 is of a fluid pinned along the edges of a corner. The interface is perturbed axially, but because the contact line is pinned, in effect, the contact angle is perturbed from the Concus-Finn condition by a small amount $\beta(z,t)$. When released the over-damped free surface will return to its original orientation due to the higher pressure on the convex side and lower pressure on the concave side of the interface. During the flow the contact angle will vary with time and location along the corner axis until equilibrium is established.

We begin the solution procedure by defining the constant height h_{cf} as measured from the corner to the free surface when $\theta = \pi/2 - \alpha$ (ref. Fig. 16). It can be shown geometrically that the relationship between h and h_{cf} is

$$h = \frac{h_{cf} \tan \alpha}{f \sin \delta}. \tag{36}$$

We can apply the perturbation through the contact angle θ such that

$$\theta(z,t) = \pi/2 - \alpha \pm \beta. \tag{37}$$

The plus or minus sign identifies either the de-wetting or wetting perturbation on the contact angle, respectively. If we expand the functions f and $\sin\delta$ in h for small β we obtain

$$h = h_{cf} \pm \beta \frac{h_{cf}\tan\alpha}{2} + O(\beta^2). \tag{38}$$

In a similar manner the area function F_A becomes

$$F_A = \tan\alpha \pm \beta \frac{1}{3}\tan^2\alpha + O(\beta^2). \tag{39}$$

Substituting h and F_A into Eq. 21 yields

$$\pm\frac{2}{3}\frac{\partial\beta}{\partial t} - \frac{\tan\alpha}{6}\beta\frac{\partial\beta}{\partial t} \mp \frac{\tan^2\alpha}{4}\beta^2\frac{\partial\beta}{\partial t} = F_i h_{cf}\left[\frac{1}{2}\frac{\partial^2\beta}{\partial z^2} \pm \frac{\tan\alpha}{3}\left(\frac{\partial\beta}{\partial z}\right)^2 \pm \frac{\tan\alpha}{3}\beta\frac{\partial^2\beta}{\partial z^2} - \frac{\tan^2\alpha}{12}\beta\left(\frac{\partial\beta}{\partial z}\right)^2 - \frac{\tan^2\alpha}{24}\beta^2\frac{\partial^2\beta}{\partial z^2} \mp \frac{\tan^3\alpha}{8}\beta^2\left(\frac{\partial\beta}{\partial z}\right)^2 \mp \frac{\tan^3\alpha}{24}\beta^3\frac{\partial^2\beta}{\partial z^2}\right]. \tag{40}$$

Applying the regular perturbation

$$\beta = \beta_0 + \epsilon\beta_1 + \epsilon^2\beta_2 + \cdots, \tag{41}$$

upon substitution into Eq. 41 the $O(1)$ equation for $\beta(z,t)$ is

$$\pm\frac{2}{3}\frac{\partial\beta_0}{\partial t} - \frac{\tan\alpha}{6}\beta_0\frac{\partial\beta_0}{\partial t} \mp \frac{\tan^2\alpha}{4}\beta_0^2\frac{\partial\beta_0}{\partial t} = F_i h_{cf}\left[\frac{1}{2}\frac{\partial^2\beta_0}{\partial z^2} \pm \frac{\tan\alpha}{3}\left(\frac{\partial\beta_0}{\partial z}\right)^2 \pm \frac{\tan\alpha}{3}\beta_0\frac{\partial^2\beta_0}{\partial z^2} - \frac{\tan^2\alpha}{12}\beta_0\left(\frac{\partial\beta_0}{\partial z}\right)^2 - \frac{\tan^2\alpha}{24}\beta_0^2\frac{\partial^2\beta_0}{\partial z^2} \mp \frac{\tan^3\alpha}{8}\beta_0^2\left(\frac{\partial\beta_0}{\partial z}\right)^2 \mp \frac{\tan^3\alpha}{24}\beta_0^3\frac{\partial^2\beta_0}{\partial z^2}\right]. \tag{42}$$

The $O(\epsilon)$ equation is

$$\pm\frac{2}{3}\frac{\partial\beta_1}{\partial t} - \frac{\tan\alpha}{6}\left(\beta_0\frac{\partial\beta_1}{\partial t} + \beta_1\frac{\partial\beta_0}{\partial t}\right) \mp \frac{\tan^2\alpha}{4}\left(\beta_0^2\frac{\partial\beta_1}{\partial t} + 2\beta_0\beta_1\frac{\partial\beta_0}{\partial t}\right) = F_i h_{cf}\left[\frac{1}{2}\frac{\partial^2\beta_1}{\partial z^2} \pm \frac{2\tan\alpha}{3}\frac{\partial\beta_0}{\partial z}\frac{\partial\beta_1}{\partial z} \pm \frac{\tan\alpha}{3}\left(\beta_0\frac{\partial^2\beta_1}{\partial z^2} + \beta_1\frac{\partial^2\beta_0}{\partial z^2}\right) - \frac{\tan^2\alpha}{12}\left(2\beta_0\frac{\partial\beta_0}{\partial z}\frac{\partial\beta_1}{\partial z} + \beta_1\left(\frac{\partial\beta_0}{\partial z}\right)^2\right) - \frac{\tan^2\alpha}{24}\left(\beta_0^2\frac{\partial^2\beta_1}{\partial z^2} + 2\beta_0\beta_1\frac{\partial^2\beta_0}{\partial z^2}\right) \mp \frac{\tan^3\alpha}{8}\left(2\beta_0^2\frac{\partial\beta_0}{\partial z}\frac{\partial\beta_1}{\partial z} + 2\beta_0\beta_1\left(\frac{\partial\beta_0}{\partial z}\right)^2\right) \mp \frac{\tan^3\alpha}{24}\left(\beta_0^3\frac{\partial^2\beta_1}{\partial z^2} + 3\beta_0^2\beta_1\frac{\partial^2\beta_0}{\partial z^2}\right)\right]. \tag{43}$$

If we note that $\beta_0 = 0$ is a solution to Eq. 42 then Eq. 43 dramatically reduces to

$$\pm\frac{2}{3}\frac{\partial\beta_1}{\partial t} = \frac{F_i h_{cf}}{2}\frac{\partial^2\beta_1}{\partial z^2}. \tag{44}$$

If we let $\tau = (F_i h_{cf} 4t)/3$ then the $O(\epsilon)$ Eq. becomes

$$\pm\frac{\partial\beta_1}{\partial\tau} = \frac{\partial^2\beta_1}{\partial z^2}. \tag{45}$$

For a single sinusoidal mode disturbance Eq. 45 can be solved and expressed to $O(\epsilon)$ as

$$\beta = \epsilon\exp[\pm\omega\tau]A\cos(\sqrt{\omega}z + B) + O(\epsilon^2). \tag{46}$$

where ω is related to both wavelength and decay rate of the perturbation and A and B are the constants determined from the boundary conditions. If we substitute Eq. 46 into Eq. 38 we can express the solution in terms of the interfacial height h as

$$h(z,\tau) = h_{cf}\left(1 \pm \epsilon\exp[\pm\omega\tau]A\cos(\sqrt{\omega}z + B)\frac{\tan\alpha}{2}\right) + O(\epsilon^2). \tag{47}$$

The $(\pm)$ symbol designates when $\beta > 0$ $(+)$ or $\beta < 0$ $(-)$, or, in other words, when the perturbation is initialized above (de-wetting) or below (wetting) the Concus-Finn condition $(\theta = \pi/2 - \alpha)$. Similar to the behavior seen in the infinite column problem, the exponent reveals the time constant,

$$\omega\tau \sim \epsilon^2\frac{3}{4}\frac{F_i h_{cf}\sin^2\alpha}{f}\frac{\sigma t}{\mu H}, \tag{48}$$

which compares with Eq. 35. Remembering that the curvature function f is positive in the wetting regime and negative in the de-wetting regime, the solution of Eq. 47 preserves the exponential decay behavior for all time as the flow settles to equilibrium. A similar perturbation solution should be possible for interfaces perturbed about any initially pinned configuration.

5 Conclusion

The interior corner flow problem is revisited and completed for partial or non-wetting fluids. Specifically in this report, the case of a retracting or de-wetting corner flow is solved above the Concus-Finn condition where $\theta \geq \pi/2 - \alpha$. Under the assumptions of a slender column, low gravity, negligible inertia and surface curvature along the flow direction, the 'cross-flow' problem must be solved in the form of a modified Poisson equation. The cross-flow problem requires the solution of the velocity distribution from which the average velocity is determined. Through a concerted choice of length scales a flow resistance function can be narrowly confined to an $O(1)$ constant. This is highly desirable to relieve undue numerical dependence in the pursuit of subsequent solutions to practical problems of interest.

In order to produce a narrowly banded flow resistance function a systematic scaling approach is pursued to determine optimal length scales x_s and y_s in the cross-flow domain. It is found that the scaling ($x_s = H$ and $y_s = H \tan\alpha$) employed in the wetting cross-flow problem also provides the narrowest flow resistance for the de-wetting problem. This result was not expected but is appreciated since dynamic flow problems can be solved and compared to the wetting corner flow solutions previously obtained by W&L [11] and others. The cross-flow problem is solved in the range of $\pi/2$ - $\alpha \leq \theta \leq \pi$. Values for F_i computed for the full range of α and θ are tabulated in the Appendices. The results produce a banded function $0.141 \lesssim F_i \lesssim 0.244$ for $\pi/2$ - $\alpha \leq \theta \leq \pi - \alpha$ which is an expanded range of the flow resistance found for the wetting section-the results being within $\pm 27\%$ when $F_i \approx 0.192$. F_i is not nearly as confined in the range of π - $\alpha \leq \theta \leq \pi$ but is still bounded. With F_i known as a weak and known $O(1)$ function for $\pi/2$ - $\alpha \leq \theta \leq \pi - \alpha$, it can be treated as a constant and implemented into a global mass balance. The result yields a second order nonlinear partial differential equation that is solved for three cases that illustrate the effectiveness of the formulation: (1) Steady flows, and (2) perturbed liquid columns including a (3) new perturbed column solution for pinned contact line conditions.

References

[1] S.F. Kistler. *Wettability*, volume 49 of *Surfactant Science Series*, chapter 6, pages 311–430. Marcel Dekker, Inc., 1993.

[2] Y. Pomeau and E. Villermaux. Two hundred years of capillarity research. *Physics Today*, pages 39–44, March 2006.

[3] R. Finn. Capillary surface interfaces. *AMS*, 46(7):770–781, August 1999.

[4] P. Concus and R. Finn. On the behavior of a capillary surface in a wedge. *Applied Mathematical Sciences*, 63:292–299, January 1969.

[5] D. Langbein. The shape and stability of liquid menisci at solid edges. *Journal of Fluid Mechanics*, 213:251–265, 1990.

[6] P.S. Ayyaswamy, I. Catton, and D.K. Edwards. Capillary flow in triangular grooves. *Journal of Applied Mechanics*, pages 332–336, June 1974.

[7] T.C. Ransohoff and C.J. Radke. Laminar flow of a wetting liquid along the corners of a predominantly gas-occupied noncircular pore. *Journal of Colloid and Interface Science*, 121(2):392–401, February 1987.

[8] L.A. Romero and F.G. Yost. Flow in an open channel capillary. *Journal of Fluid Mechanics*, 322:109–129, March 1996.

[9] R.K. Shah and A.L. London. *Laminar flow forced convection in ducts : a source book for compact heat exchanger analytical data.* Academic Press, 1978.

[10] F.M. White. *Viscous Fluid Flow.* McGraw Hill, 2nd edition, 1991. pgs. 119-121.

[11] M.M. Weislogel and S. Lichter. Capillary flow in an interior corner. *Journal of Fluid Mechanics*, 373:349–378, June 1998.

[12] M.M. Weislogel and C.L. Nardin. Capillary driven flow along interior corners formed by planar walls of varying wettability. *Microgravity Science and Technology*, XVII-3:45–55, June 2005.

[13] M.M. Weislogel. Capillary flow in interior corners: the infinite column. *Phys. Fluids*, 13(11):3101–3107, 2001.

[14] M.M. Weislogel. Capillary flow in an interior corner. *NASA*, (TM-107364), 1996.

[15] Y. Chen, M. Weislogel, and C. Nardin. Capillary driven flows along rounded interior corners. *Journal of Fluid Mechanics*, 566:235–271, April 2006.

[16] C.L. Nardin. Computation of capillary flow in interior corners: dissimilarly wetted corners and rounded corners. Master's thesis, Portland State University, 2005.

A F_i tables for corner flow

The format for Tables 2-6 follows the form shown below. Note that a dash (-) indicates a numerical solution can only be computed when θ exceeds the indicated tabular value by $\pm$ 0.03%. Note also that a * identifies when θ is within $\pm$ 0.03% for the computed F_i.

	$\cdots$	α	$\cdots$
$\vdots$		$\vdots$	
θ	$\cdots$	$F_i(\alpha, \theta)$	
$\vdots$			

Table 2: Numerical computation of F_i for α 0° to 10°

$\theta \backslash \alpha$	0.001	1	2	3	5	10
0	0.1666	0.1651	0.1636	0.1621	0.1591	0.1521
0.001	0.1666	0.1651	0.1636	0.1621	0.1591	0.1521
5	0.1666	0.1651	0.1636	0.1621	0.1592	0.1522
10	0.1666	0.1651	0.1637	0.1622	0.1593	0.1525
15	0.1666	0.1652	0.1637	0.1623	0.1595	0.1528
20	0.1666	0.1652	0.1638	0.1624	0.1597	0.1532
25	0.1666	0.1653	0.1639	0.1626	0.1599	0.1536
30	0.1666	0.1653	0.1640	0.1627	0.1602	0.1540
35	0.1666	0.1654	0.1641	0.1629	0.1604	0.1545
40	0.1666	0.1655	0.1643	0.1631	0.1607	0.1550
45	0.1666	0.1655	0.1644	0.1633	0.1610	0.1556
50	0.1666	0.1656	0.1646	0.1635	0.1614	0.1561
55	0.1666	0.1657	0.1647	0.1637	0.1617	0.1567
60	0.1666	0.1658	0.1649	0.1640	0.1621	0.1574
65	0.1666	0.1659	0.1651	0.1643	0.1625	0.1581
70	0.1666	0.1660	0.1653	0.1646	0.1630	0.1588
75	0.1666	0.1661	0.1655	0.1649	0.1635	0.1597
80	0.1666	0.1662	0.1658	0.1653	0.1641	0.1606*
85	0.1666	0.1664	0.1661	0.1658	0.1647*	0.1617
87	0.1666	0.1665	0.1663	0.1658*	0.1650	0.1621
88	0.1666	0.1665	0.1663*	-	0.1651	0.1623
89.1	0.1666	0.1666	0.1664	0.1661	0.1653	0.1626
90	0.1666	0.1667	0.1668	0.1661	0.1654	0.1628
95	0.1670	0.1672	0.1672	0.1662	0.1641	0.1641
100	0.1666	0.1672	0.1676	0.1672	0.1671	0.1656
105	0.1675	0.1681	0.1687	0.1681	0.1673	0.1673
110	0.1666	0.1678	0.1688	0.1687	0.1693	0.1692
115	0.1681	0.1694	0.1705	0.1706	0.1714	0.1714
120	0.1666	0.1686	0.1702	0.1705	0.1721	0.1739
125	0.1690	0.1712	0.1730	0.1739	0.1768	0.1768
130	0.1666	0.1696	0.1723	0.1730	0.1760	0.1802
135	0.1703	0.1736	0.1764	0.1784	0.1842	0.1842
140	0.1666	0.1711	0.1751	0.1812	0.1812	0.1888
145	0.1720	0.1769	0.1812	0.1845	0.1943	0.1943
150	0.1666	0.1731	0.1791	0.1812	0.1885	0.2008
155	0.1745	0.1817	0.1882	0.1933	0.2086	0.2086
160	0.1666	0.1762	0.1850	-	0.1991	0.2181
165	0.1783	0.1890	0.1986	0.2062	0.2296	0.2296
170	0.1666	0.1808	0.1940	0.1986	0.2151	0.2438
175	-	-	-	-	0.2261	0.2614
177	-	0.1817*	-	0.2093	0.2315*	0.2697
178	-	-	0.1977	0.2112	-	0.2740
179	-	0.1834*	-	-	0.2370	0.2790
180	0.1666	-	-	-	-	-

Table 3: F_i for α 15° to 45°

$\theta \backslash \alpha$	15	20	25	30	35	40	45
0	0.1460	0.1407	0.1363	0.1329	0.1303	0.1285	0.1275
5	0.1461	0.1409	0.1366	0.1332	0.1307	0.1291	0.1282
10	0.1464	0.1413	0.1372	0.1340	0.1316	0.1302	0.1297
15	0.1469	0.1420	0.1380	0.1349	0.1328	0.1316	0.1314
20	0.1475	0.1427	0.1388	0.1360	0.1341	0.1331	0.1331
25	0.1480	0.1434	0.1397	0.1370	0.1353	0.1345	0.1348
30	0.1487	0.1442	0.1407	0.1381	0.1365	0.1359	0.1364
35	0.1493	0.1450	0.1416	0.1392	0.1377	0.1373	0.1378
40	0.1500	0.1458	0.1425	0.1402	0.1389	0.1385	0.1392
45	0.1507	0.1466	0.1435	0.1413	0.1400	0.1398	0.1405*
50	0.1514	0.1475	0.1444	0.1423	0.1412	0.1410*	0.1418
55	0.1522	0.1484	0.1455	0.1434	0.1423*	0.1422	0.1431
60	0.1530	0.1494	0.1465	0.1446*	0.1436	0.1435	0.1444
65	0.1539	0.1504	0.1477*	0.1458	0.1448	0.1448	0.1458
70	0.1549	0.1515*	0.1489	0.1471	0.1462	0.1462	0.1472
75	0.1560*	0.1528	0.1503	0.1485	0.1477	0.1478	0.1488
80	0.1572	0.1541	0.1517	0.1501	0.1494	0.1495	0.1506
85	0.1585	0.1556	0.1534	0.1519	0.1512	0.1514	0.1525
87	0.1590	0.1563	0.1541	0.1526	0.1520	0.1522	0.1534
88	0.1593	0.1566	0.1545	0.1530	0.1524	0.1526	0.1538
89	0.1596	0.1570	0.1548	0.1534	0.1528	0.1531	0.1543
90	0.1600	0.1573	0.1552	0.1538	0.1532	0.1535	0.1547
95	0.1616	0.1592	0.1573	0.1560	0.1555	0.1559	0.1572
100	0.1635	0.1614	0.1596	0.1585	0.1581	0.1586	0.1600
105	0.1656	0.1638	0.1623	0.1613	0.1611	0.1617	0.1633
110	0.1680	0.1666	0.1653	0.1646	0.1645	0.1653	0.1670
115	0.1708	0.1697	0.1688	0.1683	0.1684	0.1694	0.1712
120	0.1740	0.1734	0.1728	0.1725	0.1729	0.1741	0.1762
125	0.1777*	0.1776	0.1774*	-	0.1781	0.1795	0.1818
130	0.1819	0.1825	0.1827	0.1832	0.1841	0.1858	0.1885
135	0.1869	-	0.1889	0.1898	0.1911	0.1932	0.1962
140	0.1927	0.1948	0.1962	0.1976	0.1993	0.2018	0.2052*
145	-	-	0.2048*	0.2067	0.2089	0.2119*	0.2158*
150	0.2078	0.2120	0.2149	0.2175	0.2203*	0.2238*	0.2283*
155	-	0.2231	0.2269	0.2302*	0.2337	0.2379*	0.2430*
160	0.2293	0.2364	0.2414	0.2456	0.2498	0.2547	0.2607*
165	0.2436	0.2525	0.2588	0.2639	0.2691*	0.2749*	0.2819*
170	0.2611*	0.2721	0.2798*	0.2862*	0.2923	0.2992	0.3074
175	0.2831*	0.2962*	0.3056	0.3132*	0.3206	0.3287	0.3384
177	0.2948*	0.3075*	0.3176	0.3258	0.3336*	0.3423*	0.3526
179	0.3038*	0.3195	0.3306	0.3395*	0.3477	0.3570	0.3681*
180	0.3096*	0.3259*	0.3373*	0.3459	0.3553	0.3648*	0.3762

Table 4: F_i for α 50° to 75°

$\theta \backslash \alpha$	50	55	60	65	70	75
0	0.1273	0.1277	0.1289	0.1307	0.1331	0.1359
5	0.1282	0.1289	0.1305	0.1330	0.1366	0.1416
10	0.1300	0.1313	0.1336	0.1371	0.1422	0.1495
15	0.1321	0.1339	0.1368	0.1412	0.1473	0.1560*
20	0.1342	0.1363	0.1398	0.1447	0.1515*	0.1610
25	0.1361	0.1386	0.1423	0.1477*	0.1549	0.1647
30	0.1379	0.1406	0.1446*	0.1502	0.1576	0.1676
35	0.1395	0.1423*	0.1465	0.1522	0.1598	0.1698
40	0.1410*	0.1439	0.1482	0.1540	0.1617	0.1716
45	0.1424	0.1454	0.1497	0.1556	0.1632	0.1730
50	0.1437	0.1468	0.1512	0.1570	0.1646	0.1743
55	0.1451	0.1482	0.1526	0.1584	0.1659	0.1755
60	0.1464	0.1495	0.1539	0.1598	0.1672	0.1766
65	0.1478	0.1510	0.1554	0.1612	0.1686	0.1779
70	0.1493	0.1525	0.1569	0.1627	0.1701	0.1793
75	0.1509	0.1541	0.1586	0.1644	0.1717	0.1810
80	0.1527	0.1560	0.1604	0.1663	0.1736	0.1829
85	0.1547	0.1580	0.1625	0.1684	0.1758	0.1851
87	0.1556	0.1589	0.1634	0.1693	0.1768	0.1861
88	0.1560	0.1594	0.1639	0.1698	0.1773	0.1866
90	0.1570	0.1603	0.1649	0.1709	0.1784	0.1877
95	0.1596	0.1630	0.1677	0.1737	0.1813	0.1908
100	0.1625	0.1660	0.1708	0.1770	0.1848	0.1944
105	0.1658	0.1695	0.1745	0.1808	0.1888	0.1987
110	0.1697	0.1736	0.1787	0.1853	0.1936	0.2038
115	0.1741	0.1782	0.1836	0.1905	0.1991	0.2097
120	0.1793	0.1836	0.1893	0.1966	0.2056	0.2167
125	0.1853	0.1899	0.1960	0.2036	0.2132	0.2347
130	0.1922	0.1972	0.2037	0.2119	0.2221	0.2347
135	0.2003	0.2058	0.2128	0.2217	0.2327	0.2462
140	0.2098	0.2158	0.2235	0.2332	0.2451	0.2599
145	0.2210	0.2276	0.2361	0.2467	0.2599	0.2762
150	0.2341*	0.2416*	0.2511	0.2629	0.2776	0.2958
155	0.2497	0.2582*	0.2688	0.2821	0.2987	0.3195
160	0.2684*	0.2780	0.2901*	0.3052*	0.3244	0.3484
165	0.2907	0.2997*	0.3156*	0.3333*	0.3556	0.3841
170	0.3176	0.3305	0.3469	0.3677	0.3943	0.4241*
175	0.3504	0.3656*	0.3851	0.4101*	0.4431	0.4871*
177	0.3654	0.3818	0.4029*	0.4302*	0.4663	0.5158*
179	0.3818*	0.3994	0.4029	0.4523*	0.4927*	0.5479*
180	0.3905	0.4089	0.4326*	0.4640*	0.5062*	0.5655

Table 5: F_i for α 80° to 90°

$\theta \backslash \alpha$	80	85	87	88	89	89.999
0	0.1388	0.1415	0.1423	0.1426	0.1427	0.1666
0.01	0.1388	0.1415	0.1423	0.1426	0.1428	-
1	0.1397	0.1444	0.1487	0.1536	0.1674*	0.2255
2	0.1416	0.1496	0.1578	0.1665*	0.1833	0.2253
3	0.1466	0.1551	0.1660*	0.1758	0.1931	0.2252
4	0.1466	0.1602	0.1724	0.1829	0.1994	0.2250
5	0.1492	0.1647*	0.1778	0.1883	0.2038	0.2284
6	0.1518	0.1687	0.1822	0.1925	0.2069	0.2248
7	0.1542	0.1722	0.1859	0.1959	0.2093	0.2246
8	0.1565	0.1753	0.1890	0.1986	0.2112	0.2244
9	0.1586	0.1780	0.1916	0.2009	0.2126	0.2243
10	0.1606*	0.1805	0.1938	0.2027	0.2138	0.2280
11	0.1625	0.1826	0.1957	0.2043	0.2148	0.2238
12	0.1642	0.1845	0.1974	0.2056	0.2156	0.2236
13	0.1658	0.1862	0.1988	0.2068	0.2162	0.2234
14	0.1673	0.1877	0.2001	0.2078	0.2168	0.2232
15	0.1687	0.1891	0.2012	0.2086	0.2172	0.2274
16	0.1700	0.1903	0.2022	0.2093	0.2175	0.2229
17	0.1712	0.1914	0.2030	0.2100	0.2178	0.2225
18	0.1723	0.1924	0.2038	0.2105	0.2180	0.2223
19	0.1733	0.1933	0.2044	0.2110	0.2182	-
20	0.1743	0.1941	0.2050	0.2114	0.2185	0.2266
21	0.1752	0.1948	0.2055	0.2117	0.2184	0.2216
22	0.1760	0.1955	0.2060	0.2120	0.2186	0.2214
23	0.1768	0.1961	0.2064	0.2123	0.2186	0.2212
24	0.1775	0.1967	0.2068	0.2125	0.2125	0.2210
25	0.1782	0.1971	0.2071	0.2127	0.2189	0.2257
30	0.1809	0.1990	0.2082	0.2133	0.2188	0.2248
35	0.1829	0.2002	0.2087	0.2135	0.2185	0.2239
40	0.1843	0.2010	0.2090	0.2134	0.2181	0.2230
45	0.1855	0.2015	0.2091	0.2133	0.2177	0.2223
50	0.1865	0.2020	0.2093	0.2133	0.2174	0.2218
55	0.1874	0.2025	0.2095	0.2133	0.2173	0.2215
60	0.1884	0.2031	0.2099	0.2136	0.2174	0.2215
65	0.1895	0.2039	0.2105	0.2141	0.2179	0.2218
70	0.1908	0.2050	0.2115	0.2150	0.2186	0.2225
75	0.1923	0.2063	0.2127	0.2163	0.2198	0.2236
80	0.1942	0.2081	0.2145	0.2179	0.2215	0.2252
85	0.1964	0.2103	0.2167	0.2201	0.2237	0.2274
90	0.1991	0.2131	0.2195	0.2229	0.2265	0.2302
91	0.1997	-	-	-	0.2268	0.2294
92	0.2003	-	-	0.2243	-	-
93	0.2010	-	0.2215	-	-	-
94	0.2017	-	-	-	-	-

Table 6: F_i for α 80° to 90° (cont.)

$\theta \backslash \alpha$	80	85	87	88	89	89.999
95	0.2023	0.2165	0.2230	0.2264	0.2297	0.2326
100	0.2062	0.2206	0.2272	0.2306	0.2341	0.2372
105	0.2108	0.2255	0.2323	0.2358	0.2393	0.2427
110	0.2162	0.2315	0.2384	0.2421	0.2458	0.2490
115	0.2227	0.2385	0.2458	0.2496	0.2534	0.2565
120	0.2303	0.2470	0.2546	0.2586	0.2627	0.2652
125	0.2394	0.2570	0.2651	0.2694	0.2733	0.2753
130	0.2501	0.2690	0.2777	0.2823	0.2864	0.2872
135	0.2629	0.2834	0.2928	0.2977	0.3022	0.3012
140	0.2781	0.3007	0.3111	0.3161	0.3213	0.3177
145	0.2965	0.3216	0.3333	0.3393	0.3450	0.3374
150	0.3186	0.3471	0.3605	0.3673	0.3740	0.3612
155	0.3456	0.3787	0.3942	0.4024	0.4098	0.3907
160	0.3790	0.4185	0.4372	0.4466	0.4545	0.4279
165	0.4210	0.4700	0.4941	0.5059	0.5162	0.4772
170	0.4753	0.5395	0.5723	0.5887	0.6024	0.5481
175	0.5485*	0.6413	0.6920	0.7208	0.7496	0.6675
177	0.5862*	0.6983*	0.7647	0.8040	0.8414	0.7518
179	0.6309*	0.7721*	0.8704*	0.9364*	1.0093	0.1203
180	0.6553*	0.8170*	0.9380*	1.0308	1.1693*	1.1203*

REPORT DOCUMENTATION PAGE		Form Approved OMB No. 0704-0188

1. REPORT DATE *(DD-MM-YYYY)*	2. REPORT TYPE	3. DATES COVERED *(From - To)*
01-09-2009	Final Contractor Report	

4. TITLE AND SUBTITLE
Capillary Corner Flows With Partial and Nonwetting Fluids

5a. CONTRACT NUMBER

5b. GRANT NUMBER
NNC05AA29A

5c. PROGRAM ELEMENT NUMBER

6. AUTHOR(S)
Bolleddula, D., A.; Weislogel, M., M.

5d. PROJECT NUMBER

5e. TASK NUMBER

5f. WORK UNIT NUMBER
WBS 825.080.04.02.20.08

7. PERFORMING ORGANIZATION NAME(S) AND ADDRESS(ES)
Portland State University
P.O. Box 751
Portland, Oregon 97207

8. PERFORMING ORGANIZATION REPORT NUMBER
E-17016

9. SPONSORING/MONITORING AGENCY NAME(S) AND ADDRESS(ES)
National Aeronautics and Space Administration
Washington, DC 20546-0001

10. SPONSORING/MONITOR'S ACRONYM(S)
NASA

11. SPONSORING/MONITORING REPORT NUMBER
NASA/CR-2009-215672

12. DISTRIBUTION/AVAILABILITY STATEMENT
Unclassified-Unlimited
Subject Categories: 28 and 34
Available electronically at http://gltrs.grc.nasa.gov
This publication is available from the NASA Center for AeroSpace Information, 443-757-5802

13. SUPPLEMENTARY NOTES

14. ABSTRACT
Capillary flow in containers or conduits with interior corners are common place in nature and industry. The majority of investigations addressing such flows solve the problem numerically in terms of a friction factor for flows along corners with contact angles *below* the Concus-Finn critical wetting condition for the particular conduit geometry of interest. This research effort provides missing numerical data for the flow resistance function F_i for partially and nonwetting systems *above* the Concus-Finn condition. In such cases the fluid spontaneously de-wets the interior corner and often retracts into corner-bound drops. A banded numerical coefficient is desirable for further analysis and is achieved by careful selection of length scales x_s and y_s to nondimensionalize the problem. The optimal scaling is found to be identical to the wetting scaling, namely $x_s = H$ and $y_s = H \tan \alpha$, where H is the height from the corner to the free surface and α is the corner half-angle. Employing this scaling produces a relatively weakly varying flow resistance F_i and for subsequent analyses is treated as a constant. Example solutions to steady and transient flow problems are provided that illustrate applications of this result.

15. SUBJECT TERMS
Fluid mechanics; Fluid flow; Capillary flow

16. SECURITY CLASSIFICATION OF:			17. LIMITATION OF ABSTRACT	18. NUMBER OF PAGES	19a. NAME OF RESPONSIBLE PERSON
a. REPORT	b. ABSTRACT	c. THIS PAGE			STI Help Desk (email:help@sti.nasa.gov)
U	U	U	UU	36	19b. TELEPHONE NUMBER *(include area code)* 443-757-5802